ACS OMEGA
http://pubs.acs.org/journal/acsodf
Article

3D-Printed Biomimetic Hierarchical Nacre Architecture: Fracture Behavior and Analysis

Jigar Patadiya, Xungai Wang, Ganapati Joshi, Balasubramanian Kandasubramanian,* and Minoo Naebe*

Cite This: *ACS Omega* 2023, 8, 18449−18461

Read Online

ACCESS | Metrics & More | Article Recommendations | SI Supporting Information

ABSTRACT: Nacreous architecture has a good combination of toughness and modulus, which can be mimicked at the micron to submicron level using 3D printing to resolve the demand in numerous applications such as automobile, aerospace, and protection equipment. The present study examines the fabrication of two nacre structures, a nacre columnar (NC) and a nacre sheet (NS), and a pristine structure via fused deposition modeling (FDM) and explores their mechanically superior stacking structure, mechanism of failure, crack propagation, and energy dissipation. The examination reveals that the nacre structure has significant mechanical properties compared to a neat sample. Additionally, NS has 112.098 J/m impact resistance (9.37% improvement), 803.415 MPa elastic modulus (11.23% improvement), and 1563 MPa flexural modulus (10.85% improvement), which are all higher than those of the NC arrangement.

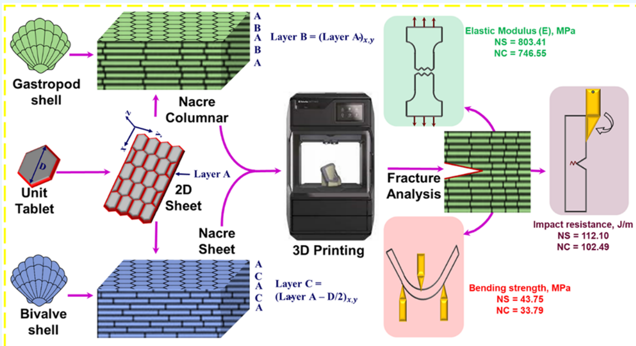

1. INTRODUCTION

Nacre, the iridescent hierarchy, yields superior mechanical performance, which is attributed to their toughening mechanisms at the micro level, such as the stacking arrangement of a tablet, the aspect ratio of a tablet, the volume fraction of hard and soft parts, and the interlocking angle, as well as at the nano level, such as nanoasperities, mineral bridges, organic interlamellar matrixes, and axial growth in the perpendicular direction.[1] Two diverse micro-architectures of nacre were found in nature known as bivalves and gastropods. The bivalve shell has a nacre sheet (NS), in which the platelets are arranged in a "brick wall" design where a mortar phase bridges the boundary among the respective underlying tiles. Columnar nacre (NC) is found in shells of gastropods, which have hexagonal platelets of almost equivalent size with matching centers that regulate the overlying tablets' nucleation.[2,3] The vigorous mechanical performance of nacre architecture relies on the accurate geometric sequencing of the tablet at the microscopic level.[4] The inner layer of mollusk shells comprises an iridescent nacre material, which has the most sought-after natural structure as it demonstrates unusual impact resistance and fracture toughness, although most of the material constitutes brittle ceramic.[5] It comprises 95 wt % brittle aragonite platelets, calcium carbonate ($CaCO_3$) crystal form, and a 5 wt % soft phase of polysaccharides and protein, forming a nanostructure of brick-and-mortar arrangement. The bricks are densely packed with polygonal aragonites of 5−8 μm diameter and 20−90 Å thick platelets and welded by the mortar matrix of organic interlamellar of 1−5 Å thickness.[6,7] This distinctive hierarchical building could be the basis of protective equipment and body armor with numerous functions, including high strength, lightweight, high energy absorbing capacity, and high stiffness due to its equally 3 times superior energy absorption associated with the fundamental composites.[8] Nacre columnar (NC) comprises almost uniform tablets which regulate the nucleation site of the overlying tablets as centers are overlapping, whereas in a NS, a "brick wall" pattern is followed for tablet stacking, and deposition starts over most of the inner surface of the shell.[9] The top view of the columnar nacre has revealed that the adjacent layers intersect and represent polygonal tablets in such a way that the lamellar interfaces are perpendicular to inter-platelet borders, which form tessellated bands on the other hand in NS geometry; the distributions of inter-tablet boundaries are random.[10] The overlap and core regions are significant in the NC because the stress experienced in both areas varies. In the NS, the core and overlap regions experience no distinction.[11,12] Nacre can achieve remarkable toughness and strength simultaneously, employed in diverse structural applications like aerospace and automotive, based on the loading direction and fracture mechanism. NC has well-defined deformation bands that are perpendicular to the loading

Received: December 20, 2022
Accepted: April 13, 2023
Published: May 15, 2023

https://doi.org/10.1021/acsomega.2c08076
ACS Omega 2023, 8, 18449−18461

direction of the columnar structure, and NS forms an unusual network of deformation bands at an angle to the main crack.[13] The research focuses on developing artificial nacre structures with strengthening mechanisms, such as crack blunt, deflection, stress delocalization, crack bridging, interfacial strengthening, topological interlocking, and aspect ratio[14,15] to accomplish the requirements of high structural applications. Researchers have studied the fracture modes and gained an understanding of the failure of the nacre using simulation and analytical modeling approaches; nevertheless, there have not been many experimental studies conducted to understand the observed behavior.[16−18] Modern manufacturing methods, such as 3D printing, open room to designing bio-inspired artificial nacre materials with systematic control over brick-and-mortar stacking, interlocking, toughening, and failure understanding.[19,20] Additive manufacturing (AM) enables on-demand customized construction of the object by virtue of 3D scan's digital slicing, CAD, or tomography data, where substances form layer-by-layer, devoid of the demand for machining and molds. AM techniques covered numerous categories per ISO/ASTM 59200:2021 based on the feeding material type or curing mechanisms. Existing AM technologies include extrusion (Fused deposition modeling (FDM), 3D dispensing, direct ink writing (DIW), 3D plotting, and 3D fiber deposition), vat photopolymerization [stereolithography (SLA) and digital light processing (DLP)], powder bed fusion [selective laser sintering (SLS) and selective laser melting (SLM)], binder jetting (3D bioprinting, aerosol 3D printing, and inkjet), material jetting, sheet lamination (LOM), and direct energy deposition (DED).[21] The working principle, pertinent features, advantages, and limitations are covered in Table 1 and portrayed in Figure 1. FDM, fused filament fabrication (FFF), DIW, 3D dispensing, and 3D bio plotting fall into the material extrusion category where feedstock is particularly dispensed in an $x-y$ plane through a heated nozzle with a predefined diameter, as described in Figure 1.[22] Extrusion-based AM involves printing of thin thread in a predefined first-layer pattern, followed by subsequent layer deposition (downward movement of platform in the z-axis) until the desired 3D piece is obtained[23,24] (Figure 1a,b). Transformation of a liquid photopolymer to a solid object by application of a light source falls under the category of vat polymerization, where ultra-high molecular-weight monomer or oligomer material is reticulated using ultraviolet light. SLA and DLP are two sub-categories of vat polymerization (Figure 1c). First-layer adhesion with a platform or solidification of resin initiated at a specific depth with a precise geometrical pattern via a light beam from laser. After curing of the initial layer, the building stage is shifted downward for another liquid filling and second layer reticulation; subsequently, other layers are added until the defined height.[25] In the material jetting process (Figure 1d), the photopolymer droplets of specific shape are selectively deposited on a platform using one or more mobile printing heads. To facilitate a uniform and continuous flow of material during the injection process, the viscosity of material is reduced using heating and later deposited material is cured through a UV light beam. The drop deposition method permits accurate aligning of the material, providing high tolerance to the body under the building and reducing material waste. Powder-based AM begins by conveying a powder layer material from the materials feed platform to the printing stage using feeding rollers.[26] Fusion (in binder jetting, Figure 1e) or sintering (in SLS, SLM,

Table 1. Summary of Various Printing Technologies with Their Features, Merits, and Demerits[a]

type of 3D printing	material used	solidification mechanism	feature resolution (μm)	pros	cons
vat polymerization	photosensitive resins, acrylates, epoxides	photopolymerization	25−100	high resolution, precision, and surface quality	photo processing is necessary; objects are vulnerable to weak and heat
extrusion-based	soft polymers, thermoplastics, inks, PLA, ABS, PC, composites	sequencing layered cooling at moderate and room temperature	100−150	excellent strength component reduces the cost of production, versatility in material selection	a sluggish process, high roughness, high processing temperature
powder-based fusion	PA12, PEEK, ceramics, metal, alloys	sintering, melting	50−100	a robust and complex part, less anisotropy	rough surfaces; poor Reusability of unsintered powder
material or binder jetting	dielectric starch, conductive inks, gels	crosslinking of polymers, room temperature cooling	10−25	multimaterial, fast printing, low-temperature process	low viscous ink needed, limited strength of the part, low surface finish
sheet lamination	PVC, paper, plastic sheet	laser cutting and binder curing via laser	200−300	compact desktop printing	high anisotropy, low resolution, limited materials
DED	metal powder pr wire	laser sintering or melting	150−200	more complex design printing, any shape building, low material waste	expensive, low resolution, surface finish
3D bioprinting	thermoplastics, composites, photoresins, hydrogels, biomaterials	UV curing, crosslinking curing at an average temperature	10−100	a broad range of materials	narrow viscosity process window

[a]Reused from refs 21 and 29 with permission. Copyright 2017 & 2021, ACS.

https://doi.org/10.1021/acsomega.2c08076
ACS Omega 2023, 8, 18449−18461

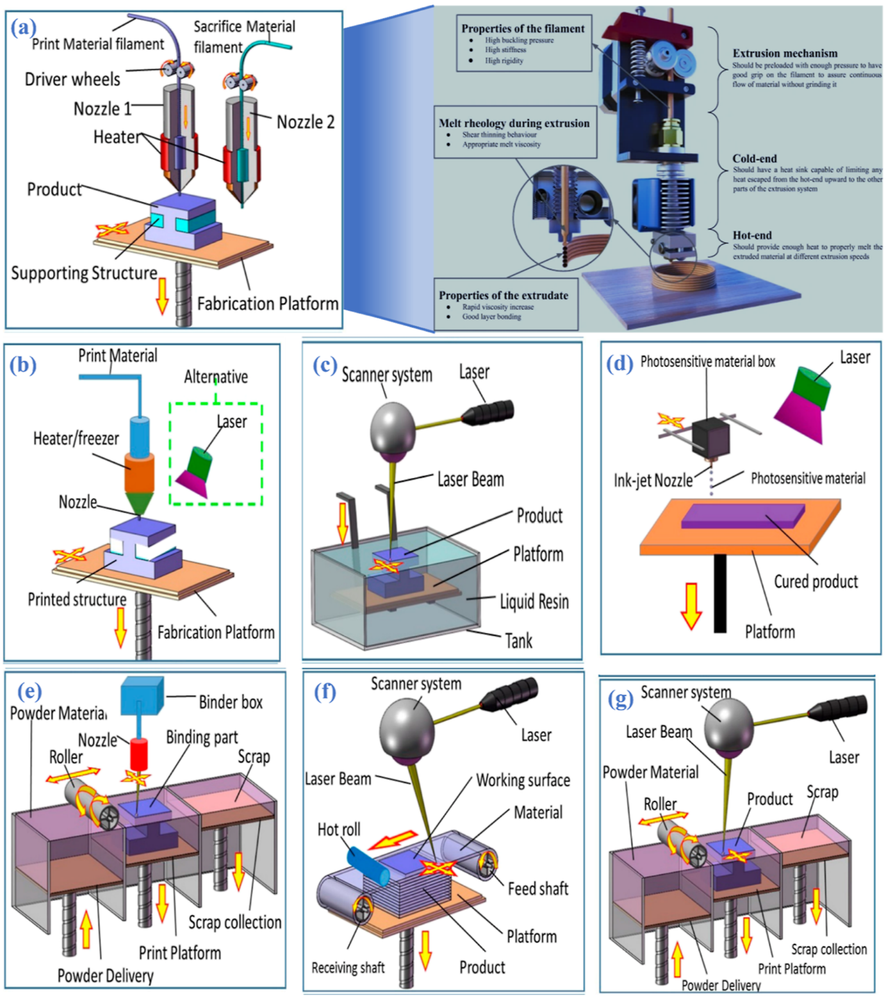

Figure 1. Graphic representation of numerous 3D printing processes. (a) extrusion-based FDM with its features and proper extrusion, (b) extrusion-based DIW process, (c) SLA method of liquid resin, (d) photopolymerization in Polyjet, (e) 3D modeling via binder jetting, (f) sheet lamination process (LOM), and (g) method of SLM and SLS. Reused from refs 30 and 31 with permission: Copyright 2017, MDPI, and Copyright 2021, Springer Nature.

and EBM, Figure 1g) of the powder material to a desired shape is accomplished by a programed energy source or binder deposition to the platform surface. This step is repeated to obtain the final 3D geometry, and further post-processing is performed to eliminate the infiltrated or support material.[27] The sheet lamination printing technique can be employed to construct three-dimensional (3D) pieces from continuous cutting of 2D sections followed by lamination. This AM method can be classified into two, unrolled and rolled procedures linked by a sheet of material piloted by the revolving rollers. Deeding and storing of material are simultaneously performed in this system. In addition, sheet lamination has a printing stage (that can execute vertical changes), a roller, and a laser[28] (Figure 1f).

FDM demonstrates an encouraging route among all 3D-printing manufacturing techniques to facilitate direct incorporation of the intricate, micro-level, multi-material, and porous geometries within the final 3D object.[32] FFF and FDM are widely utilized techniques among other 3D printing techniques that permit the adequate printing of intricate constructions guided by XYZ movement according to CAD models. Over traditional manufacturing, the key advantages of the FDM technique are that it enables rapid prototyping and on-demand fabrications. Moreover, FDM is at the lead of facilitating restructured production, which is crucial to diminishing the carbon footprint and empowering smart production approaches in the upcoming market.[23] Though effective in building satisfactory erections, compared with FDM, the existing volumetric AM technologies, SLA, and DLP printing have a low utilization efficiency of wet material (the weight proportion of the final fabricated architecture to the original quantity of liquid resin in a bath). Other than this, they have less utilization efficiency of the remaining material (the weight proportion of the attained dry printed geometry to the initial quantity of liquid resin).[33] Aspects of FDM printing and processing parameters such as building speed and improving the accuracy, functionality, mechanical properties, porosity, surface finish, and stability are addressed.[34] Versatile applications establish how FDM-based AM has been developed for energy technology, lightweight engineering, optics, architecture, food processing, drug delivery, dentistry, and personalized medicine.[35] The collection of polymeric materials used in FDM encompasses materials like polymer blends, thermoplastics, functional polymers, elastomers, hydrogels, biological systems, and composites. FDM uses most thermoplastic materials, such as polylactic acid (PLA),

https://doi.org/10.1021/acsomega.2c08076
ACS Omega 2023, 8, 18449−18461

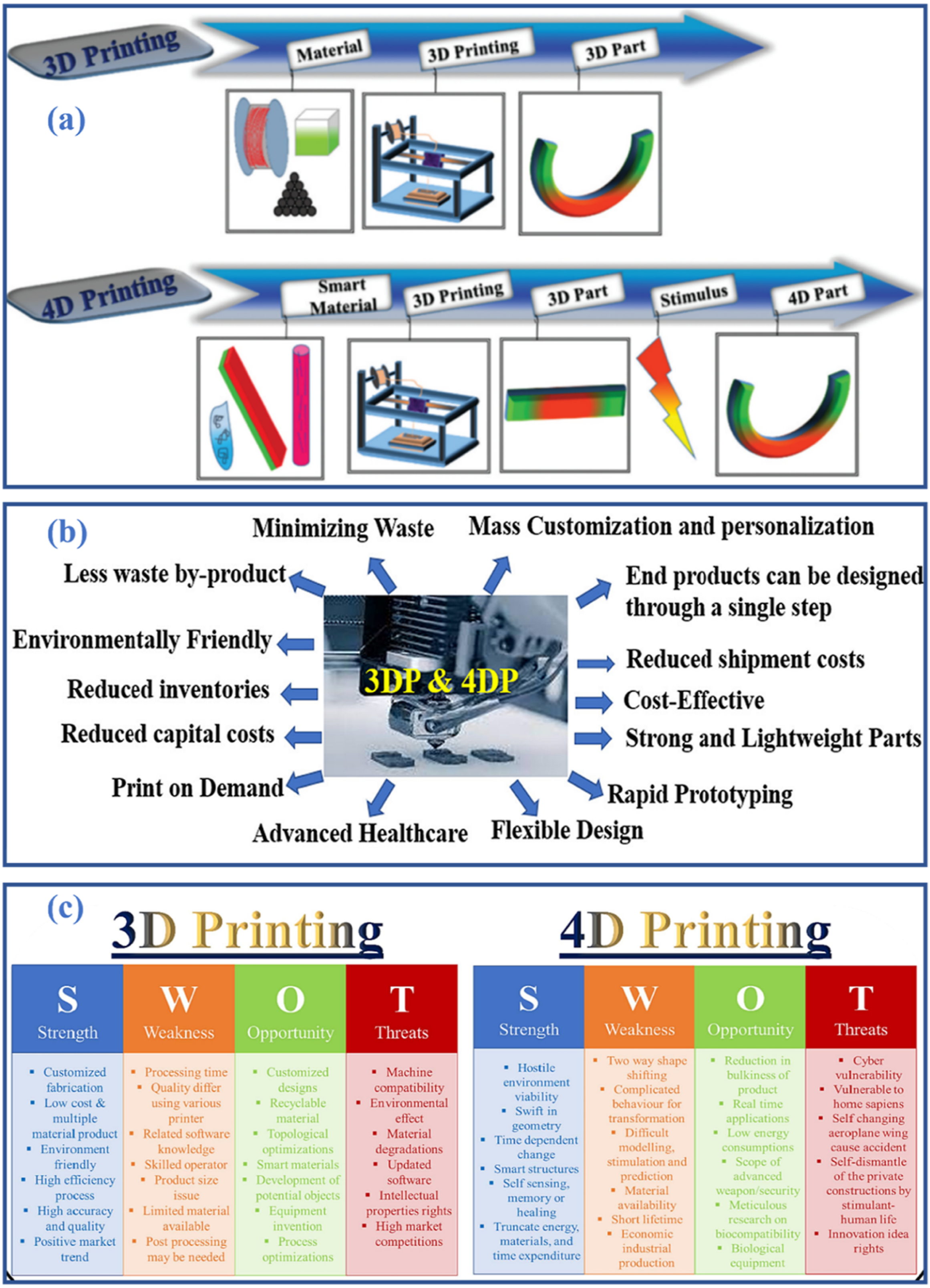

Figure 2. (a) Difference between the 3D and 4D printing processes and output. Reused from ref[22] with permission. Copyright 2021, Taylor & Francis, (b) General advantages and disadvantages achieved by 3D and 4D printing technology. Reprinted from ref[48] with permission. Copyright 2022, Elsevier. (c) SWOT analysis for both techniques. Adapted from ref[46] with permission. Copyright 2023, Elsevier.

acrylonitrile butadiene styrene (ABS), nylon, polyethylene terephthalate glycol, and their blends like polycarbonate−ABS (PC-ABS), nylon carbon fibers in the form of the continuous diameter filament.[20,36] Apart from conventional materials, filaments are produced with reinforced composites to enhance thr mechanical properties, non-flammability, chemical stability, and high abrasion. Wang et al. evaluated a high-performance PEEK composite reinforced with the carbon fiber (CF) and

Table 2. Comparison of 3D and 4D Printing with Different Materials, Designs, Changes Undergone (if Any), and Applications[a]

	3D printing	4D printing
materials	thermoplastics, metals, ceramics, biomaterials, or nanomaterials	self-assembled materials, multi-materials designed materials examples: shape memory alloy/polymer/hybrids, self-degradation/deformation materials, temperature/UV-driven materials
design	3D digital information	3D digital information for change
printer	3D printer examples: SLA, material extrusion, and SLS	smart 3D printer examples: modified nozzle, binder, and laser multimaterial 3D printer examples: solid/liquid, solid/solid, gradient materials, and nanocomposites
static or astatic	as printed/static	After printing changes in shape, color functions over time
applications	jewelery, toys, fashion, entertainment, automobiles, aerospace, defense, and bio/medical devices	applications involved a dynamic change in configurations

[a]Reused from[47] with permission. Copyright 2020, Elsevier.

glass fiber (GF). The investigation indicated that incorporation of CF and GF from 5 to 15 wt % improved the thermal properties, mechanical characteristics (flexural properties are 5 wt % GF/PEEK (165 MPa) and 5 wt % CF/PEEK (94 MPa), with the improvement of 17% and 19% over that of produced pure PEEK, respectively), and surface porosity.[37] A mechanical attribute of an object significantly differs from bulk material or input material properties, in which adhesive bonding creates each layer from the extruded fiber's connection. Layered fabrication depends on various property-controllable characteristics like direction of the printing layer, raster angle, infill pattern, and infill direction, which untimely result in either being brittle or ductile depending on the combination of printing parameters.[38] Josef Kiendl investigated that incorporating a brittle PLA material in FDM-printed objects renders brittle behavior in the parallel printing direction to the loading direction, while the inclined direction of printing to loading results in ductile behaviour.[39] Consequently, many of the researchers have established numerous nature-inspired hierarchies, including a mollusk shell layer of nacreous material, utilizing filament-based AM and verifying the modification in structural characteristics. Peng and co-workers designed fused deposition-modeled biomimetic architecture to mimic Elytrigia repens and examined the resilience and stiffness through mechanical analysis and multiscale finite element analysis (FEA).[40] Jia et al. created numerous nature-inspired constructions, through multi-material FDM printing for the compact tension (CT) fracture test. They estimated the toughness for fracture employing a nonlinear elastic *J*-integral approach and evaluated the mechanisms of toughening using fracture theories.[41] Padole et al. fabricated a range of biomimetic structures, including NC and NS, prismatic, complex cross lamellar, and foliated structures using FDM-based 3D printing. The result of their study shows that, owing to the well-defined hierarchical architecture, superior toughness and extraordinary impact strength were observed in the nacreous structure among the produced architectures.[3] Yadav et al., developed nature-inspired materials by mimicking the architecture of molluscan shells, such as complex cross lamellae, foliated, cross-lamellae, and nacre, using a layer-by-layer FDM printing technique. They concluded each constituent affected the mechanical and surface frictional properties according to structural manipulation.[42] Ko et al. designed the nacre-mimicked architecture to fabricate an optimum impact resistance under three various impact conditions through an integrative utilization of bi-material 3D printing, drop-weight impact test, parametric study, and FEA.[43]

3D printed materials are not limited to static nature but can be reformed by shifting distinct characteristics, such as shape, hardness, color, functions, and transparency, when subjected to heat, magnetic or electrical source, water, pH, and light, which is an advance form of 3D printing known as 4D printing[44,45] (Figure 2a). 3D- and 4D-printed composites cover vital applications in mechanical constructions, in aeronautical, automotive, consumer goods, and aviation industries, and in sports or safety equipment. The prime benefits of 3D and 4D printing technologies are that they have fewer waste materials, require less energy during manufacturing, and have extreme flexibility in the fabrication related to conventional techniques; therefore, both the printing techniques have tremendous potential for innovation, design, and development in various sectors[46,47] (Figure 2b,c). A recapitulation of 3D/4D printing based on innovation, materials employed, and changes in printed objects, printers, and applications is presented in Table 2.

The present investigation focuses on an experimental comparison of FDM-printed artificial nacre structures concerning different stacking arrangements, columnar nacre, and sheet nacre. The monolithic Polycarbonate-Acrylonitrile Butadiene Styrene (PC-ABS) was chosen for the experiment because it provides excellent processibility and heat distortion resistance and exhibits good impact resistance, improved shrinkage, and dimensional stability. The mechanical response via the Izod impact test, tensile test, and flexural bending testing elucidated NS's superior stress-distributing capability compared to NC erection. Therefore, our report comparing the performance of different nacreous structures shows the experimental validation and potentially broadens the feasible fabrication route of NS and NC architectures.

2. MECHANISM OF NACRE FRACTURE

The natural organic region in the hierarchy behaves as a multidomain structure of adhesion binding in-between aragonite ceramic platelets, which provides good energy dissipation in every ceramic platelet delamination. It has been contemplated that the aragonite plates exhibit ductile attributes when perpendicular to the direction of applied strain renders. Additionally, Gries and co-workers revealed the existence of holes with the width of 2.5 and 38.4 nm in the aragonite region and considered that the presence of voids diminishes the propagation of the crack, thus enhancing the fracture toughness of shells.[49] Besides that, Xia and the team established that controlled sliding of nanoasperities renders an unusual mechanical behavior to strain hardening.[50] Chen and

https://doi.org/10.1021/acsomega.2c08076
ACS Omega 2023, 8, 18449−18461

colleagues presented five mechanisms for nacre toughening: (1) weak organic interface, (2) interlocking of nanoasperities, (4) inter-lamellar mineral bridges, (4) plastic deformation of individual tiles, (5) numerous cracks, and enormous-scale crack bridging[51] (Figure 3). Nacre fracture is further reduced

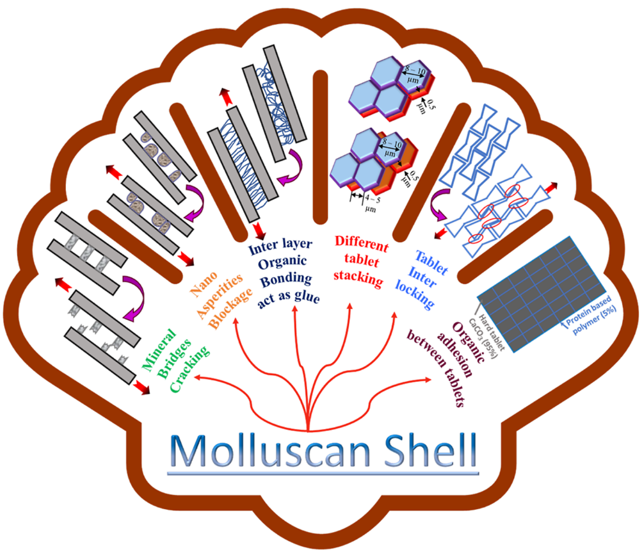

Figure 3. Illustration of various fracture mechanisms in the nacreous mollusk shell, the mother-of-pearl.

by adding nanoasperities, voids, pre-strain, cracks, mineral bridges, and soft materials with long polymeric chains.[52] The composite of nacre hierarchy can be directly applied in materials currently employed in structural components due to they demonstrate length scales and polymer chemistry analogous to those of traditional fiber-reinforced polymers. The high stiffness, toughness, and strength of these nature-inspired materials could be readily applied, such as in the leading edge of aircraft foils, or protective layers in turbine blades, to locally diminish abrasion, damage by impact, and surface wear in these vital structural applications. On the other hand, the chemistry between organic and inorganic region could be altered to generate resorbable and osteoinductive hierarchical materials for application in regeneration of bone.[53,54] This experiment focused on ballistic performance to characterize nacre composite using the following parameters crucial in determining the impact energy absorption.[43] Consequently, the absorbed impact energy by the fabricated Nacre-like structure "e" can be mathematically formulated by a function of the dimensional parameters as,[43]

$$e = f(A_M, A_B, v_i, D_i, m_i, \rho_c, E_c, \sigma_{yc}, I_c) \tag{1}$$

where A_M and A_B represent the areas of mortar and brick, respectively, ρ_c Is the density of the composite, E_c and σ_{yc} are the composite's elastic modulus and yield strength, and I_c describes the Izod strength of the composite. A nacre-like composite comprised an equal number of fundamental dimensions and repeating variables, with three essential dimensions and ten repeating variables. Therefore, seven pi equations were possible as the impact velocity v_i, the diameter of the impactor D_i, and the impactor's mass m_i have all dimensional components.

$$\pi_1 = [m_i]^\alpha [D_i]^\beta [V_i]^\gamma [\mathrm{e}] \tag{2}$$

$$\pi_2 = [m_i]^\alpha [D_i]^\beta [V_i]^\gamma [A_{TPU}] \tag{3}$$

$$\pi_3 = [m_i]^\alpha [D_i]^\beta [V_i]^\gamma [A_{PLA}] \tag{4}$$

$$\pi_4 = [m_i]^\alpha [D_i]^\beta [V_i]^\gamma [\rho_c] \tag{5}$$

$$\pi_5 = [m_i]^\alpha [D_i]^\beta [V_i]^\gamma [E_c] \tag{6}$$

$$\pi_6 = [m_i]^\alpha [D_i]^\beta [V_i]^\gamma [\sigma_{yc}] \tag{7}$$

$$\pi_7 = [m_i]^\alpha [D_i]^\beta [V_i]^\gamma [I_c] \tag{8}$$

The exponents are independent variables described by α, β, and γ and from eq 1 dimensional parameters can be written in terms of fundamental physical units mass M, length L, and time T, $[e] = \mathrm{ML^2\,T^{-2}}$, $[A_{TPU}] = [A_{PLA}] = \mathrm{L^2}$, $[v_i] = \mathrm{LT^{-1}}$, $[D_i] = \mathrm{L}$, $[m_i] = \mathrm{M}$, $[\rho_c] = \mathrm{ML^{-3}}$, $[E_c] = [\sigma_{yc}] = \mathrm{ML^{-1}\,T^{-2}}$, and $[I_c] = \mathrm{MT^{-2}}$. Solving all the nondimensional pi equations from (2) to (8) derivation gives

$$\pi_1,\ [m_i]^{\alpha+1}[D_i]^{\beta+2+\gamma}[V_i]^{-2-\gamma} = 0 \tag{9}$$

$$\pi_2,\ [m_i]^{\alpha}[D_i]^{2+\beta+\gamma}[V_i]^{-\gamma} = 0 \tag{10}$$

$$\pi_3,\ [m_i]^{\alpha}[D_i]^{2+\beta+\gamma}[V_i]^{-\gamma} = 0 \tag{11}$$

$$\pi_4,\ [m_i]^{1+\alpha}[D_i]^{-3+\beta+\gamma}[V_i]^{-\gamma} = 0 \tag{12}$$

$$\pi_5,\ [m_i]^{1+\alpha}[D_i]^{-1+\beta+\gamma}[V_i]^{-2-\gamma} = 0 \tag{13}$$

$$\pi_6,\ [m_i]^{1+\alpha}[D_i]^{-1+\beta+\gamma}[V_i]^{-2-\gamma} = 0 \tag{14}$$

$$\pi_7,\ [m_i]^{1+\alpha}[D_i]^{\beta+\gamma}[V_i]^{-2-\gamma} = 0 \tag{15}$$

Nondimensional variables can be derived as follows because the dimensions in eqs 9−15 are zero

$$\pi_1 = \frac{e}{m_i v_i^2} \tag{16}$$

$$\pi_2 = \frac{A_{TPU}}{D_i^2} \tag{17}$$

$$\pi_3 = \frac{A_{PLA}}{D_i^2} \tag{18}$$

$$\pi_4 = \frac{\rho_c D_i^3}{m_i} \tag{19}$$

$$\pi_5 = \frac{E_c D_i^3}{m_i v_i^2} \tag{20}$$

$$\pi_6 = \frac{\sigma_{yc} D_i^3}{m_i v_i^2} \tag{21}$$

$$\pi_7 = \frac{I_c D_i^3}{m_i v_i^2} \tag{22}$$

where π_1 represents the ratio of energy absorbed to the kinetic energy of the projectile, π_2 represents the zone ratio of the soft matrix and the zone of the impactor, π_3 is the contact area ratio of the complex phase and impactor area, π_4 indicates the percentage mass per volume of composites to the impactor

https://doi.org/10.1021/acsomega.2c08076
ACS Omega 2023, 8, 18449−18461

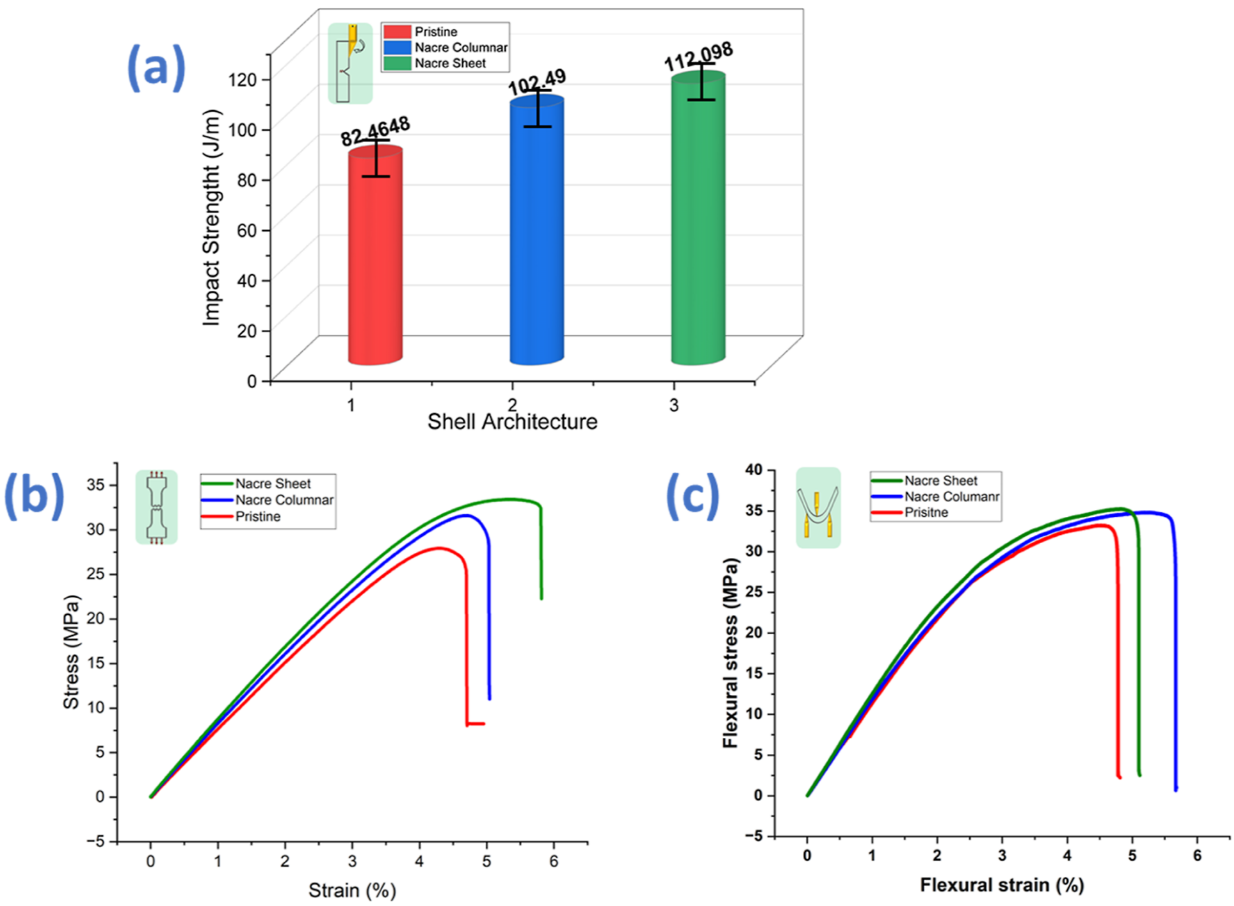

Figure 4. Mechanical testing results of (a) Izod impact test, (b) tensile test, and (c) flexural bending test.

density, π_5 represent elastic modulus vs dynamic energy per volume, π_6 is a ratio of strength at a yield to vibrant energy per volume, π_7 indicates the ratio of Izod impact strength vs kinetic energy per volume.

The fracture of nacre materials relies on a stiff and stacking arrangement, the shape and size of a tablet, volume fraction of tablet (hard) material and organic (soft) material, the interlocking angle, aspect ratio, and mineral bridges. However, numerous analytical and simulation studies were conducted to examine failure behavior and superior mechanical structure concerning stacking arrangements in NC and NS. The crack propagation, crack hindering, and braking of these significant uniform and nonuniform placements in NC and NS were represented by various models like (i) discrete element method (DEM),[18] (ii) representative volume element (RVE),[17] and (iii) trans-scale shear-lag model.[16] The study showed using DEM (eqs 23−25) that the propagation of a crack in NC is through the tablet boundary, which can be hindered and pinned; nevertheless, a slight amount increases in toughness; as a result, it will reduce the cohesive length of pinning compared to the coherent size of the crack. On the other hand, NS structure crack propagation was uneven, and pinning at many stages improved the mechanical strength and toughness.

Moreover, the developed NC model shows all junctions open, conveying linear deformation and sliding of the tablet during RVE analysis. In contrast, the NS model exhibits a stair pattern where a large number of intersections remain closed or partially open.[17] More explanation regarding analytical and simulation models for the fracture of different stackings in nacre will be found in Supporting Information file S1.

$$\text{bridging model toughness, } J_B = k\ \rho\ J_{i,}\ \text{normalised toughness} = \frac{J}{J_B} \tag{23}$$

$$\text{tablet aspect ratio, } \rho = L/t, \text{ specific aspect ratio} = \bar{\rho} \tag{24}$$

$$\text{crack extension} = \Delta\alpha/t \tag{25}$$

3. METHODOLOGY

Artificial nacre is manufactured via PC-ABS owing to an appropriate impact strength of 25.5 kJ/m^2, tensile strength of 37 MPa, low density of 1.1 g/cm^3, high flow, and Vicat softening temperature 108 °C. FDM (Method X, MakerBot) was used to fabricate a shell architecture with 100% infill density and a 0.1 mm layer height. Characterizing intricate nacre geometry analyzed using an Izod impact tester (Tinius Olsen Impact 503) as per ASTM D256, tensile testing, and 3-point flexural bending test (UTM. Instron) performed according to ASTM D638 and ASTM D790 accordingly. The microstructure examination of fractured hierarchical and cryogenic fractures was analyzed using FESEM (Zeiss, Germany). The surface roughness of FDM-printed components was quantified using RUGOSURF 90G surface rough-

https://doi.org/10.1021/acsomega.2c08076
ACS Omega 2023, 8, 18449−18461

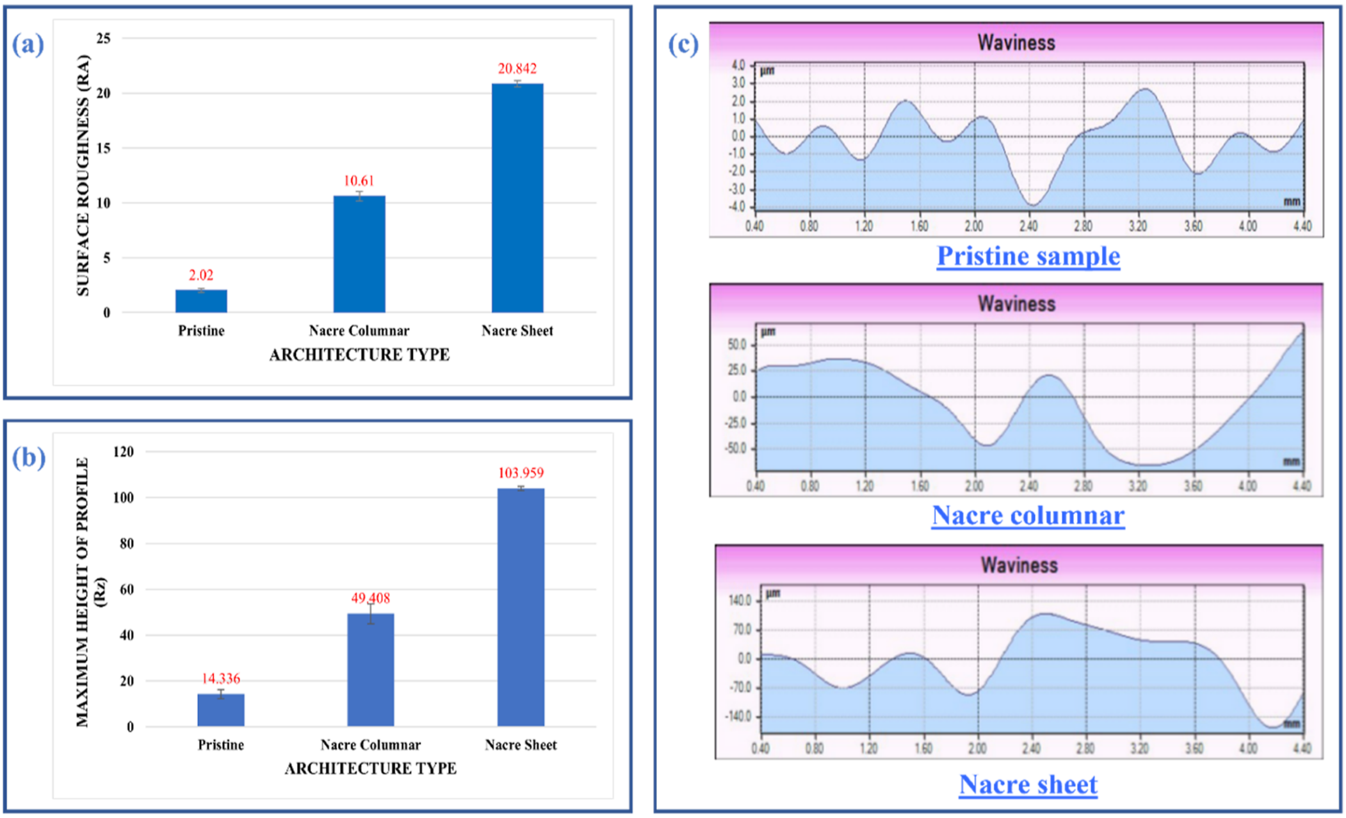

Figure 5. Representation of surface roughness evolution results, (a) surface roughness, R_A value of three different arrangements, (b) maximum height of top layer profile, R_z value, and (c) surface waviness graphs of pristine, NC, and NS geometry.

ness testers (TESA SWISS MAKE) for pure and nacre parts to estimate the surface imperfection considering different designs. The mean surface roughness (Ra) and the mean maximum height of the profile (Rz) are quantified for the upper surface layer of the FDM-printed neat PCABS, columnar, and sheet samples. Three different regions on a sample were assessed for roughness of the surface in each arrangement.

4. RESULTS AND DISCUSSION

The impact resistance was performed as per ASTM D256, where the specimen was designed via Solid Works, followed by fused deposition 3D printing of PC-ABS. According to the NS and NC, the prepared specimens had different stacking arrangements, tablet interfaces, and tablet locking from each other. Therefore, each sample noticeably comprises a varied capacity for absorbing impact energy.[43] Figure 3a delineates identical features of the printed nacre composite, where the impact resistance (IR) and absorb energy (AE) of the NS system (AE = 0.7323 J) was thought to be uppermost in addition to the supreme energy absorption of the NC skeleton (AE = 0.6106 J) compared to the monolithic PC-ABS sample (AE = 0.5457 J). The toughness of mollusk shells is attributed (deformation and fracture) to various mechanisms comprising void formation, nanoasperities, and their controlled sliding, interlocking of a tablet, and interlayer mineral bridges.

Meanwhile, the developed nacre architecture does not encompass either interlocking, mineral bridges, or nano-hierarchy; consequently, the impact performance could be a function of the tablet's center direction and its configurations.[55] Figure 4a delineated the average value of five sequential experiments for impact resistance and absorb energy. Furthermore, tensile testing was conducted as per the ASTM D638 type IV standards for PC-ABS printed samples, which boosted the experimental and analytical study on NC and NS. It was evident from the survey that crack propagation, while fracture in mollusk shell follows numerous methodologies; however, the phenomenon of stress whitening or process zone was observed in the energy dissipation mechanism of nacre, which is equivalent to the polymeric systems crazing.[56] Following that, Figure 4b deduces the tensile characteristics of advanced composites, where the initial stress−strain curve indicates an almost equivalent nature to yielding or low-strain applications.

Additionally, promoting further load on structures, NS manifests a noteworthy enhancement in force dissipation up to 33.3897 MPa of ultimate stress, although NC ends at 31.5986 MPa and the clean sample reached 27.9189 MPa. In contrast, Young's modulus (E) of the NS (803.42 MPa) describes a superior value to the NC (746.55 MPa) sequentially compared to the pristine structure (623.33). As per the RVE model, a similar behavior shows that under the action of uniaxial force, cracks propagate in the direction that grips low energy; hence, a NC skeleton made of uniform stacking yields a crack deflection path, while at the same point, breaks encounters with hard bricks in an asymmetrical network, which urges for surpassing energy in NS.

Additionally, Figure 4c also provides the load−displacement curve of dynamic mechanical flexural bending flexural results of monolithic, NC, and sheet architecture.[57] As per Figure 4c, from the initial loading until the fracture, the NC structure deforming slightly subordinately corresponds to a non-uniformed nacre array, whereas the pristine geometry trails

https://doi.org/10.1021/acsomega.2c08076
ACS Omega 2023, 8, 18449−18461

Figure 6. Design of NC and NS architectures. (a) design of the single tablet, a 2D sheet of brick-and-mortar phase, CAD model of NC and sheet, and 3D printed view (expanded top view); (b) fracture surface morphology of pristine, columnar, and sheet structure analysis using an optical microscope and SEM images with a specific region of hard (brick) and soft (mortar) segments.

an identical path. For columnar stacking, the crack propagates at the interface of brick, which can be separated quickly, leading to crazing in the zone, while the sheet also has an equivalent tendency to a generation of crack, yet the propagation hinders subsequent bricks in layered position. The bending strengths of 3D-printed immaculate geometry and gastropod architecture achieved the maximum levels of 32.05 and 33.79 MPa, respectively, whereas bivalve shell geometry reached the ultimate power of 43.75 MPa. However, it has been noticed that total energy absorbance capacity was superior for the NC, attributed to minor interlayer deviation and interface tablet cohesion against bending load conditions.[58]

The surface unevenness value of the upper layer of PCABS objects is calculated, and the mean average of surface roughness (Ra) and the mean maximum profile height (Rz) for each bio-inspired skeleton are provided in Figure 5a,b. As per shown in Figure 5c for the 2D roughness profiles, it is observed that the roughness profile is higher if the peak-to-valley difference is height, which is described by the nacreous sheet; however, it progressively declines for columnar nacre and a neat sample.[59] The new PCABS component comprises an R_A value (arithmetic average) of 2.02 μm and an R_Z value of 14.336 μm; nonetheless, for the NC structure, a maximum R_A reaches 11.038 μm, and a value of R_Z observed as 49.408 μm and the highest surface roughness R_A of 20.842 μm, and R_Z of 103.959 μm are obtained for densely packed NC tablets. Printing top layer patterns such as 0/90, −45/+45, hexagonal, and concentric have voids and porosity, which act as unevenness in the outermost layers, increasing roughness. Chemical treatments in 3D printing modify the top surface due to dissolving surface material and filling the voids between rasters, resulting in a smoother and more uniform surface. Surface texture is a surface roughness component that plays a crucial role in defining the composite interaction with other environments such as temperature, water, coatings, and adhesives. Roughness is an excellent gauge of the prospective functioning of a mechanical component owing to irregularities on the plane that could form a nucleation site for corrosion or cracks.[60,61]

Combining the high toughness and strength of nacre-like 2D sheets can be achieved by blocking crack propagation along the platelet side and the interface in their nanostructure of brick-and-mortar. Although the variation of cracks in the micro-structure of brick-and-mortar is well detailed, numerous other mechanisms for energy absorption in bio-inspired materials can exist.[62] Numerical connections between bulk, micro-, and nanostructures revealed the microscopic effect on mechanical performance. While a crack propagates in locally disordered zones, the crack is pinned and generates stress concentration around that zone. These hurdles to crack propagation are either bunches of platelet unevenness or greater-than-mean platelets concerning most of the platelets. Such microstructural divergencies are, therefore, crucial to inhibiting crack propagation in nacre-like geometries.[63,64] There are various computation models to predict fracture behavior, toughening mechanisms, and microstructural change during loadings like the cohesive finite-element method, MD simulation, Monte Carlo simulation, DEM, representative volume element, FEA, and trans-scale shear-lag model.[65−67] The nacre hierarchy was

https://doi.org/10.1021/acsomega.2c08076
ACS Omega 2023, 8, 18449−18461

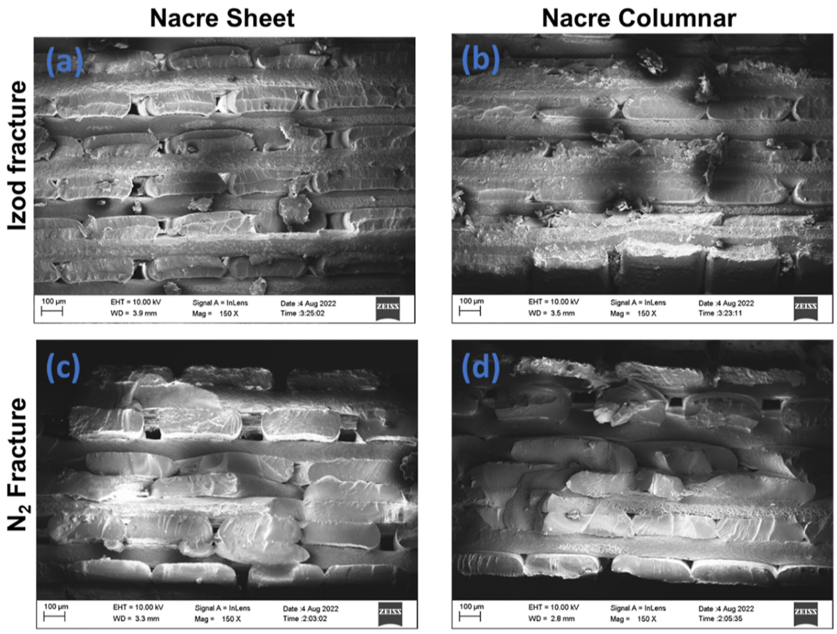

Figure 7. FESEM images of NS and NC for (a,b) Izod and (c,d) cryogenic fracture.

produced as a 3D brick and mortar model for both sheet and columnar and fractured evolute using the optical microscopic image and SEM to study the surface morphology of fabricated samples, as illustrated in Figure 6. It has been expansively studied that the glassy polymers' failure process largely relies on shear banding or crazing (microscopic) or necking (macroscopic) flow, and it scatters the constrained stress via cavitation, bond rupture, viscoelastic deformation, crack growth, and crazing before catastrophic material failure. The SEM analysis of ruptured PCABS parts has proved their distinctive fracture mechanics, that is, the interlayer raster delamination, multiple crazing, and shear deformation mechanism.[68,69] The FDM-printed nacre design revealed the nonregular contiguity formation between the layers of PCABS samples; however, such structural local imperfection does not relinquish any compromise in the impact resistance compared to the neat PCABS sample. As mentioned above, mollusk structure follows various methodologies for dissipating energy during cracking. Nevertheless, Barthelat illuminated that the "process zone" known as "stress whitening" was exhibited in nacreous architectures during the fracture process. Such an exterior surface fracture is equivalent to crazing in polymeric systems.[42,56]

Moreover, FESEM micrographs of microstructure observations concerning Izod and cryogenic fracture surfaces are elucidated in Figure 7. Impact fracture of NS and NC articulated architecture is coined as a non-brittle failure phenomenon that exhibits a tearing surface that involves crazing and cavitation phenomena of plastic deformation. Additionally, liquid nitrogen-dipped fracture of NS and NC, evident interlayer crack propagation, and cracked delocalization result in energy dissipation, presumably without interfacial debonding.[42]

PC/ABS composites are known for their excellent mechanical properties, thermal stability, extrudability, and poor biodegradation due to inadequate PC and ABS links. The structural properties of PC/ABS cannot be altered using mechanical or chemical separation, so the utilization of this composite is highly beneficial for structural applications. On the other hand, the decomposition of the PCABS composite was conducted using pyrolysis, where heating in the presence of various catalysts and bromine was generally combined with solid residues or pyrolysis oil. It is essential to utilize feasible methods to decompose PCABS components to obtain dibrominated products without catalysts or additives.[35,70,71] Li and Xu applied a supercritical water oxidation process for environmentally friendly and efficient decomposition where depolymerization, conjugation of free radicals, carbonization, and generation of free radicals could be the mechanism.[72]

5. CONCLUSIONS

Nacre has remarkable resistance to impact load due to the distinctive hierarchy created by the two diverse contrasting arrangements: the unidirectional tablet stacking columnar and an angular tablet organized sheet. By controlling the proportions of the intermediate component (soft phase), the augmented resistance of impact, elastic and flexural modulus, and strength of the unique nacre-like compounds could be attained. The aragonite phase is surrounded by biopolymeric materials and entails a brick-and-mortar microarchitecture in a lamellar manner with tremendous energy dissipation during rupture. The biomineralization process of nacre occurs in a bottom-up approach, which can be mimicked using a similar bottom-up fabrication tool, such as FDM, a 3D printing technique. Organic−inorganic bonding, tablet size, interlocking, tablet distribution, volumetric percentage of soft and hard phases, and intra-layer adhesion are crucial to strengthening fracture resistance in an artificial nacre. This study demonstrates a unified approach to identifying and validating numerous analytic and simulation models of NC and NS. We first utilized dimensionless parameters and analytical models to illustrate the stacking of geometry, characteristics of the material, and mechanical response of the nacre-like composites for 3D design. The designed models were fabricated via FDM printing with the PC-ABS filament in a brick-and-mortar manner. We envisioned that the NS structure with the same other parameters, excluding stacking, was superior in impact, tensile, and bending properties. The

https://doi.org/10.1021/acsomega.2c08076
ACS Omega 2023, 8, 18449−18461

mechanical behavior of NS structures showed improvement of 9.37% in impact resistance, 11.23% in elastic modulus, and 10.85% in flexural modulus as compared to NC, while 36, 29, and 37% improvements in impact, elastic modulus, and flexural modulus, respectively, were noticed in contrast to pure geometry. Nacre design structures can be applied as bulk implants, coatings, inflammable films, structural components, or composite components when merged with ceramics and other polymeric materials.

■ ASSOCIATED CONTENT

Supporting Information

The Supporting Information is available free of charge at https://pubs.acs.org/doi/10.1021/acsomega.2c08076.

Brief description of analytical, numerical, and simulation models such as DEM, RVE, and Monte Carlo for determining the fracture, crack propagation, and toughening mechanism of mollusk seashell nacreous hierarchy (PDF)

■ AUTHOR INFORMATION

Corresponding Authors

Balasubramanian Kandasubramanian − *Additive Manufacturing Laboratory, Department of Metallurgical and Materials Engineering, Defence Institute of Advanced Technology (DU), Pune 411025 Maharashtra, India;* orcid.org/0000-0003-4257-8807; Email: meetkbs@googlemail.com

Minoo Naebe − *Institute for Frontier Materials, Deakin University, Geelong, Victoria 3216, Australia;* orcid.org/0000-0002-0607-6327; Email: minoo.naebe@deakin.edu.au

Authors

Jigar Patadiya − *Institute for Frontier Materials, Deakin University, Geelong, Victoria 3216, Australia; Additive Manufacturing Laboratory, Department of Metallurgical and Materials Engineering, Defence Institute of Advanced Technology (DU), Pune 411025 Maharashtra, India*

Xungai Wang − *JC STEM Lab of Sustainable Fibers and Textiles, School of Fashion and Textiles, The Hong Kong Polytechnic University, Kowloon, Hong Kong;* orcid.org/0000-0002-3549-6769

Ganapati Joshi − *Additive Manufacturing Laboratory, Department of Metallurgical and Materials Engineering, Defence Institute of Advanced Technology (DU), Pune 411025 Maharashtra, India*

Complete contact information is available at: https://pubs.acs.org/10.1021/acsomega.2c08076

Notes

The authors declare no competing financial interest.

■ ACKNOWLEDGMENTS

The authors acknowledge research support from DIAT (DU) and Deakin University, Australia, under the Deakin India Research Initiative (DIRI). The corresponding author wishes to dedicate this paper to Prof. Dwarkanath D Kale, retired professor of technology of plastic, UDCT, Mumbai, Matunga, Maharashtra. The authors are grateful to and acknowledge the efforts and consideration of Dr. Robin McIntyre, D. Phil, Director, Iconiq Innovation, Leicestershire, United Kingdom, in improving the technicality and refining the English language of the manuscript. The first author acknowledges NMRL and ARDE (DRDO) labs, Bhushan Lokhande, Amol Indalkar, and all the lab members of the AM lab, DIAT (DU), for their continuous and valuable technical support throughout the research and writing. The first author wishes to acknowledge Keyur Chovatiya for design support, Dr. Amrita Nighojkar, Niranjana J.P., Alsha Subash, Neelaambhigai Mayilswamy, and Alok Kumar for their continuous motivation and support. The authors are thankful to the editor and anonymous reviewers who have helped improve the manuscript's quality.

■ REFERENCES

(1) Mishra, N.; Kandasubramanian, B. Biomimetic Design of Artificial Materials Inspired by Iridescent Nacre Structure and Its Growth Mechanism. *Polym. Plast. Technol. Eng.* **2018**, *57*, 1592−1606.

(2) Yadav, R.; Naebe, M.; Wang, X.; Kandasubramanian, B. Review on 3D Prototyping of Damage Tolerant Interdigitating Brick Arrays of Nacre. *Ind. Eng. Chem. Res.* **2017**, *56*, 10516−10525.

(3) Padole, M.; Gharde, S.; Kandasubramanian, B. Three-Dimensional Printing of Molluscan Shell Inspired Architectures via Fused Deposition Modeling. *Environ. Sci. Pollut. Res.* **2020**, *28*, 46356−46366.

(4) Sun, J.; Bhushan, B. Hierarchical Structure and Mechanical Properties of Nacre: A Review. *RSC Adv.* **2012**, *2*, 7617−7632.

(5) Burns, L.; Mouritz, A. P.; Pook, D.; Feih, S. Bio-Inspired Hierarchical Design of Composite T-Joints with Improved Structural Properties. *Compos. B Eng.* **2015**, *69*, 222−231.

(6) Wang, Y.; Xia, S.; Li, H.; Wang, J. Unprecedentedly Tough, Folding-Endurance, and Multifunctional Graphene-Based Artificial Nacre with Predesigned 3D Nanofiber Network as Matrix. *Adv. Funct. Mater.* **2019**, *29*, 1903876.

(7) Yang, Y.; Li, X.; Chu, M.; Sun, H.; Jin, J.; Yu, K.; Wang, Q.; Zhou, Q.; Chen, Y. Electrically Assisted 3D Printing of Nacre-Inspired Structures with Self-Sensing Capability. *Sci. Adv.* **2019**, *5*, No. eaau9490.

(8) Rodrigues, J. R.; Alves, N. M.; Mano, J. F. Nacre-Inspired Nanocomposites Produced Using Layer-by-Layer Assembly: Design Strategies and Biomedical Applications. *Mater. Sci. Eng. C* **2017**, *76*, 1263−1273.

(9) Yourdkhani, M.; Pasini, D.; Barthelat, F. Multiscale Mechanics and Optimization of Gastropod Shells. *J. Bionic Eng.* **2011**, *8*, 357−368.

(10) Tang, B.; Niu, S.; Yang, J.; Shao, C.; Wang, M.; Ni, J.; Zhang, X.; Yang, X. Investigation of Bioinspired Nacreous Structure on Strength and Toughness. *Biomimetics* **2022**, *7*, 120.

(11) Chen, W.; Zhang, P.; Yu, S.; Zang, R.; Xu, L.; Wang, S.; Wang, B.; Meng, J. Nacre-Inspired Underwater Superoleophobic Films with High Transparency and Mechanical Robustness. *Nat. Protoc.* **2022**, *17*, 2647−2667.

(12) Du, F.; Alghamdi, S.; Yang, J.; Huston, D.; Tan, T. Interfacial Mechanical Behavior in Nacre of Red Abalone and Other Shells: A Review. *ACS Biomater. Sci. Eng.* **2022**, DOI: 10.1021/acsbiomaterials.2c00080.

(13) Rabiei, R.; Bekah, S.; Barthelat, F. Failure Mode Transition in Nacre and Bone-like Materials. *Acta Biomater.* **2010**, *6*, 4081−4089.

(14) Cui, S.; Lu, Z.; Yang, Z. Effect of Interlocking Structure on Mechanical Properties of Bio-Inspired Nacreous Composites. *Compos. Struct.* **2019**, *226*, 111260.

(15) Ubaid, J.; Wardle, B. L.; Kumar, S. Bioinspired Compliance Grading Motif of Mortar in Nacreous Materials. *ACS Appl. Mater. Interfaces* **2020**, *12*, 33256−33266.

(16) Hansong, M.; Yueguang, W.; Jingru, S.; Lihong, L. Mechanical Behavior and Size Effect of the Staggered Bio-Structure Materials. *Mech. Mater.* **2018**, *126*, 47−56.

(17) Rabiei, R.; Bekah, S.; Barthelat, F. Failure mode transition in nacre and bone-like materials. *Acta Biomater.* **2010**, *6*, 4081−4089.

(18) Abid, N.; Pro, J. W.; Barthelat, F. Fracture Mechanics of Nacre-like Materials Using Discrete-Element Models : Effects of Microstructure , Interfaces and Randomness. *J. Mech. Phys. Solids* **2019**, *124*, 350−365.

(19) Liu, F.; Li, T.; Jia, Z.; Wang, L. Combination of Stiffness, Strength, and Toughness in 3D Printed Interlocking Nacre-like Composites. *Extreme Mech. Lett.* **2020**, *35*, 100621.

(20) Kim, Y.; Jeong, H.; Gu, G. X.; Ryu, S. A Three-Dimensional Fracture Pattern Diagram of Staggered Platelet Structures. *Compos. Struct.* **2019**, *220*, 769−775.

(21) Ligon, S. C.; Liska, R.; Stampfl, J.; Gurr, M.; Mülhaupt, R. Polymers for 3D Printing and Customized Additive Manufacturing. *Chem. Rev.* **2017**, *117*, 10212−10290.

(22) Patdiya, J.; Kandasubramanian, B. Progress in 4D Printing of Stimuli Responsive Materials. *Polym.-Plast. Technol. Mater.* **2021**, *60*, 1845−1883.

(23) Cano-Vicent, A.; Tambuwala, M. M.; Hassan, S. S.; Barh, D.; Aljabali, A. A. A.; Birkett, M.; Arjunan, A.; Serrano-Aroca, Á. Fused Deposition Modelling: Current Status, Methodology, Applications and Future Prospects. *Addit. Manuf.* **2021**, *47*, 102378.

(24) Mercado Rivera, F. J.; Rojas Arciniegas, A. J. Additive Manufacturing Methods: Techniques, Materials, and Closed-Loop Control Applications. *Int. J. Adv. Manuf. Technol.* **2020**, *109*, 17−31.

(25) Li, Y.; Wang, W.; Wu, F.; Kankala, R. K. Vat Polymerization-Based 3D Printing of Nanocomposites: A Mini Review. *Front. Mater.* **2023**, *9*, 9.

(26) Mora, S.; Pugno, N. M.; Misseroni, D. 3D Printed Architected Lattice Structures by Material Jetting. *Mater. Today* **2022**, *59*, 107−132.

(27) Han, W.; Kong, L.; Xu, M. Advances in Selective Laser Sintering of Polymers. *Int. J. Extreme Manuf.* **2022**, *4*, 042002.

(28) El Awad Azrak, S. M.; Clarkson, C. M.; Moon, R. J.; Schueneman, G. T.; Youngblood, J. P. Wet-Stacking Lamination of Multilayer Mechanically Fibrillated Cellulose Nanofibril (CNF) Sheets with Increased Mechanical Performance for Use in High-Strength and Lightweight Structural and Packaging Applications. *ACS Appl. Polym. Mater.* **2019**, *1*, 2525−2534.

(29) Patadiya, J.; Gawande, A.; Joshi, G.; Kandasubramanian, B. Additive Manufacturing of Shape Memory Polymer Composites for Futuristic Technology. *Ind. Eng. Chem. Res.* **2021**, *60*, 15885−15912.

(30) Xu, Y.; Wu, X.; Guo, X.; Kong, B.; Zhang, M.; Qian, X.; Mi, S.; Sun, W. The Boom in 3D-Printed Sensor Technology. *Sensors* **2017**, *17*, 1166.

(31) Shaqour, B.; Abuabiah, M.; Abdel-Fattah, S.; Juaidi, A.; Abdallah, R.; Abuzaina, W.; Qarout, M.; Verleije, B.; Cos, P. Gaining a Better Understanding of the Extrusion Process in Fused Filament Fabrication 3D Printing: A Review. *Int. J. Adv. Manuf. Technol.* **2021**, *114*, 1279−1291.

(32) Alarifi, I. M. Mechanical Properties and Numerical Simulation of FDM 3D Printed PETG/Carbon Composite Unit Structures. *J. Mater. Res. Technol.* **2023**, *23*, 656−669.

(33) Zhang, Y.; Dong, Z.; Li, C.; Du, H.; Fang, N. X.; Wu, L.; Song, Y. Continuous 3D Printing from One Single Droplet. *Nat. Commun.* **2020**, *11*, 4685.

(34) Joseph, B.; Ninan, N.; Visalakshan, R. M.; Denoual, C.; Bright, R.; Kalarikkal, N.; Grohens, Y.; Vasilev, K.; Thomas, S. Insights into the Biomechanical Properties of Plasma Treated 3D Printed PCL Scaffolds Decorated with Gold Nanoparticles. *Compos. Sci. Technol.* **2021**, *202*, 108544.

(35) Oladapo, B. I.; Oshin, E. A.; Olawumi, A. M. Nanostructural Computation of 4D Printing Carboxymethylcellulose (CMC) Composite. *Nano-Struct. Nano-Objects* **2020**, *21*, 100423.

(36) Serjouei, A.; Yousefi, A.; Jenaki, A.; Bodaghi, M.; Mehrpouya, M. 4D Printed Shape Memory Sandwich Structures: Experimental Analysis and Numerical Modeling. *Smart Mater. Struct.* **2022**, *31*, 055014.

(37) Wang, P.; Zou, B.; Ding, S.; Huang, C.; Shi, Z.; Ma, Y.; Yao, P. Preparation of Short CF/GF Reinforced PEEK Composite Filaments and Their Comprehensive Properties Evaluation for FDM-3D Printing. *Compos. B Eng.* **2020**, *198*, 108175.

(38) Gottschalk, N.; Bogdahn, M.; Harms, M.; Quodbach, J. Brittle Polymers in Fused Deposition Modeling: An Improved Feeding Approach to Enable the Printing of Highly Drug Loaded Filament. *Int. J. Pharm.* **2021**, *597*, 120216.

(39) Kiendl, J.; Gao, C. Controlling Toughness and Strength of FDM 3D-Printed PLA Components through the Raster Layup. *Compos. B Eng.* **2020**, *180*, 107562.

(40) Peng, M.; Wen, Z.; Xie, L.; Cheng, J.; Jia, Z.; Shi, D.; Zeng, H.; Zhao, B.; Liang, Z.; Li, T.; Jiang, L. 3D Printing of Ultralight Biomimetic Hierarchical Graphene Materials with Exceptional Stiffness and Resilience. *Adv. Mater.* **2019**, *31*, 1902930.

(41) Jia, Z.; Wang, L. 3D Printing of Biomimetic Composites with Improved Fracture Toughness. *Acta Mater.* **2019**, *173*, 61−73.

(42) Yadav, R.; Goud, R.; Dutta, A.; Wang, X.; Naebe, M.; Kandasubramanian, B. Biomimicking of Hierarchal Molluscan Shell Structure Via Layer by Layer 3D Printing. *Ind. Eng. Chem. Res.* **2018**, *57*, 10832−10840.

(43) Ko, K.; Lee, S.; Hwang, Y. K.; Jin, S.; Hong, J. W. Investigation on the Impact Resistance of 3D Printed Nacre-like Composites. *Thin-Walled Struct.* **2022**, *177*, 109392.

(44) Rastogi, P.; Gharde, S.; Kandasubramanian, B. *Thermal Effects in 3D Printed Parts*, 2020, pp 43−68. DOI: 10.1007/978-981-15-5424-7_3.

(45) Korde, J. M.; Kandasubramanian, B. Fundamentals and Effects of Biomimicking Stimuli-Responsive Polymers for Engineering Functions. *Ind. Eng. Chem. Res.* **2019**, *58*, 9709−9757.

(46) Patadiya, J.; Naebe, M.; Wang, X.; Joshi, G.; Kandasubramanian, B. Emerging 4D Printing Strategies for On-Demand Local Actuation & Micro Printing of Soft Materials. *Eur. Polym. J.* **2023**, *184*, 111778.

(47) Subash, A.; Kandasubramanian, B. 4D Printing of Shape Memory Polymers. *Eur. Polym. J.* **2020**, *134*, 109771.

(48) Ameta, K. L.; Solanki, V. S.; Singh, V.; Devi, A. P.; Chundawat, R. S.; Haque, S. Critical Appraisal and Systematic Review of 3D & 4D Printing in Sustainable and Environment-Friendly Smart Manufacturing Technologies. *Sustainable Mater. Technol.* **2022**, *34*, No. e00481.

(49) Gries, K.; Kröger, R.; Kübel, C.; Fritz, M.; Rosenauer, A. Investigations of Voids in the Aragonite Platelets of Nacre. *Acta Biomater.* **2009**, *5*, 3038−3044.

(50) Xia, S.; Wang, Z.; Chen, H.; Fu, W.; Wang, J.; Li, Z.; Jiang, L. Nanoasperity: Structure Origin of Nacre-Inspired Nanocomposites. *ACS Nano* **2015**, *9*, 2167−2172.

(51) Chen, Q.; Pugno, N. M. Bio-Mimetic Mechanisms of Natural Hierarchical Materials: A Review. *J. Mech. Behav. Biomed. Mater.* **2013**, *19*, 3−33.

(52) Grossman, M.; Bouville, F.; Masania, K.; Studart, A. R. Quantifying the Role of Mineral Bridges on the Fracture Resistance of Nacre-like Composites. *Proc. Natl. Acad. Sci. U.S.A.* **2018**, *115*, 12698−12703.

(53) Xin, Z.; Zhang, X.; Duan, Y.; Xu, W. Nacre-Inspired Design of CFRP Composite for Improved Energy Absorption Properties. *Compos. Struct.* **2018**, *184*, 102−109.

(54) Grossman, M.; Pivovarov, D.; Bouville, F.; Dransfeld, C.; Masania, K.; Studart, A. R. Hierarchical Toughening of Nacre-Like Composites. *Adv. Funct. Mater.* **2019**, *29*, 1806800.

(55) Dimas, L. S.; Bratzel, G. H.; Eylon, I.; Buehler, M. J. Tough Composites Inspired by Mineralized Natural Materials: Computation, 3D Printing, and Testing. *Adv. Funct. Mater.* **2013**, *23*, 4629−4638.

(56) Barthelat, F.; Tang, H.; Zavattieri, P. D.; Li, C. M.; Espinosa, H. D. On the Mechanics of Mother-of-Pearl: A Key Feature in the Material Hierarchical Structure. *J. Mech. Phys. Solids* **2007**, *55*, 306−337.

(57) Wu, X.; Meng, X.; Zhang, H. An experimental investigation of the dynamic fracture behavior of 3D printed nacre-like composites. *J. Mech. Behav. Biomed. Mater.* **2020**, *112*, 104068.

https://doi.org/10.1021/acsomega.2c08076
ACS Omega 2023, 8, 18449−18461

(58) Mohamed, O. A.; Masood, S. H.; Bhowmik, J. L. Analysis of Wear Behavior of Additively Manufactured PC-ABS Parts. *Mater. Lett.* **2018**, *230*, 261−265.

(59) Sammaiah, P.; Rushmamanisha, K.; Praveenadevi, N.; Rajasri Reddy, I. The Influence of Process Parameters on the Surface Roughness of the 3d Printed Part in FDM Process. *IOP Conf. Ser. Mater. Sci. Eng.* **2020**, *981*, 042021.

(60) Jayanth, N.; Senthil, P.; Prakash, C. Effect of Chemical Treatment on Tensile Strength and Surface Roughness of 3D-Printed ABS Using the FDM Process. *Virtual Phys. Prototyp.* **2018**, *13*, 155−163.

(61) Fernández, S.; Jiménez, M.; Porras, J.; Romero, L.; Espinosa, M. M.; Domínguez, M. Additive Manufacturing and Performance of Functional Hydraulic Pump Impellers in Fused Deposition Modeling Technology. *J. Mech. Des.* **2016**, *138*, 024501.

(62) Bouville, F.; Maire, E.; Meille, S.; Van de Moortèle, B.; Stevenson, A. J.; Deville, S. Correction: Corrigendum: Strong, Tough and Stiff Bioinspired Ceramics from Brittle Constituents. *Nat. Mater.* **2017**, *16*, 1271.

(63) Huang, Z.; Li, X. Origin of Flaw-Tolerance in Nacre. *Sci. Rep.* **2013**, *3*, 1693.

(64) Saad, H.; Douillard, T.; Malchère, A.; Steyer, P.; Meille, S.; Deville, S.; Reynard, B. Toughening Mechanisms in Nacre-like Alumina Revealed by in-Situ Imaging of Stress. *J. Eur. Ceram. Soc.* **2022**, *42*, 6757−6761.

(65) Raj, M.; Patil, S. P.; Markert, B. Mechanical Properties of Nacre-Like Composites: A Bottom-Up Approach. *J. Compos. Sci.* **2020**, *4*, 35.

(66) Li, Y.; Zhou, M. Prediction of Fracture Toughness of Ceramic Composites as Function of Microstructure: I. Numerical Simulations. *J. Mech. Phys. Solids* **2013**, *61*, 472−488.

(67) Lim, R. K.; Pro, J. W.; Begley, M. R.; Utz, M.; Petzold, L. R. High-Performance Simulation of Fracture in Idealized 'Brick and Mortar' Composites Using Adaptive Monte Carlo Minimization on the GPU. *Int. J. High Perform. Comput. Appl.* **2016**, *30*, 186−199.

(68) Wu, X.; Meng, X.; Zhang, H. An Experimental Investigation of the Dynamic Fracture Behavior of 3D Printed Nacre-like Composites. *J. Mech. Behav. Biomed. Mater.* **2020**, *112*, 104068.

(69) Naebe, M.; Abolhasani, M. M.; Khayyam, H.; Amini, A.; Fox, B. Crack Damage in Polymers and Composites: A Review. *Polym. Rev.* **2016**, *56*, 31−69.

(70) Adhikari, J.; Perwez, M. S.; Das, A.; Saha, P. Development of Hydroxyapatite Reinforced Alginate−Chitosan Based Printable Biomaterial-Ink. *Nano-Struct. Nano-Objects* **2021**, *25*, 100630.

(71) Yan, X.; Bethers, B.; Chen, H.; Xiao, S.; Lin, S.; Tran, B.; Jiang, L.; Yang, Y. Recent Advancements in Biomimetic 3D Printing Materials With Enhanced Mechanical Properties. *Front. Mater.* **2021**, *8*, 518886.

(72) Li, K.; Xu, Z. Decomposition of Polycarbonate/Acrylonitrile-Butadiene-Styrene Blends in e-Waste Packaging Resin and Recovery of Debrominated Carbon Materials by Supercritical Water Oxidation Process. *J. Hazard. Mater.* **2021**, *404*, 124056.

https://doi.org/10.1021/acsomega.2c08076
ACS Omega 2023, 8, 18449−18461